NANO LETTERS

Letter

pubs.acs.org/NanoLett

Evolution of Electronic Structure as a Function of Layer Thickness in Group-VIB Transition Metal Dichalcogenides: Emergence of Localization Prototypes

Lijun Zhang*,†,‡ and Alex Zunger*,†

†University of Colorado, Boulder, Colorado 80309, United States

‡College of Materials Science and Engineering, Jilin University, Changchun 130012, China

Supporting Information

ABSTRACT: Layered group-VIB transition metal dichalcogenides (with the formula of MX_2) are known to show a transition from an indirect band gap in the thick n-monolayer stack $(MX_2)_n$ to a direct band gap at the n = 1 monolayer limit, thus converting the system into an optically active material suitable for a variety of optoelectronic applications. The origin of this transition has been attributed predominantly to quantum confinement effect at reduced n. Our analysis of the evolution of band-edge energies and wave functions as a function of n using ab initio density functional calculations including the long-range dispersion interaction reveals (i) the indirect-to-direct band gap transformation is triggered not only by (kinetic-energy controlled) quantum confinement but also by (potential-energy controlled) band repulsion and localization. On its own, neither of the two effects can explain by itself the energy evolution of the band-edge states relevant to the transformation; (ii) when n decreased, there emerge distinct regimes with characteristic localization prototypes of band-edge states deciding the optical response of the system. They are distinguished by the real-space direct/indirect in combination with momentum-space direct/indirect nature of electron and hole states and give rise to distinct types of charge distribution of the photoexcited carriers that control excitonic behaviors; (iii) the various regimes associated with different localization prototypes are predicted to change with modification of cations and anions in the complete MX_2 (M = Cr, Mo, W and X = S, Se, Te) series. These results offer new insight into understanding the excitonic properties (e.g., binding energy, lifetime etc.) of multiple layered MX_2 and their heterostructures.

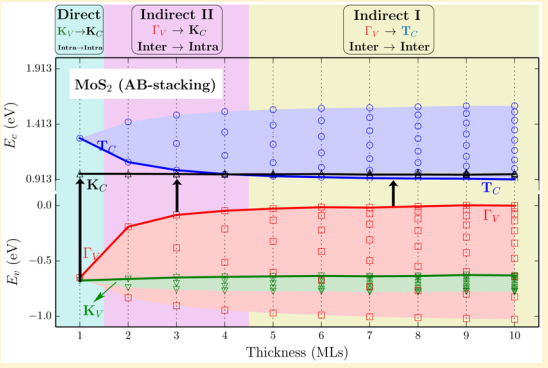

KEYWORDS: *Transition metal dichalcogenides, molybdenum disulfide, indirect-to-direct band gap transition, excitons*

Different Momenta and Spatial Localization of the Electronic States Involved in Light Absorption. Layered group-VIB transition metal dichalcogenides (TMDs) with MoS_2 as the prototype material have attracted considerable interest for a variety of potential optoelectronic applications[1−3] because of the wide tunability of their electronic properties offered by control of structural parameters such as the layer thickness,[4−7] stacking pattern of multiple layers,[8−11] or applied strain[12−17] and external fields.[18,19] Among these control knobs, particular attention has recently been focused on the transformation of the indirect band gap in multiple-layered thick films to a direct gap at the monolayer (ML) limit,[4−7,20,21] thus conversing the system from an optically inactive material to a strong light absorber. This is illustrated by Figure 1a showing the indirect gap transition of bulk MoS_2, connecting the valence band maximum (VBM) at the wave vector Γ (denoted as Γ_V) to the conduction band minimum (CBM) at T (located between Γ and K and denoted as T_C), whereas in the monolayer MoS_2 (Figure 1b) the band gap is direct with the VBM and CBM both located at K (denoted as K_v and K_c, respectively). The direct/indirect features of this transformation are described in terms of momentum conserving in the k-space. However, in addition to this "k-space direct/indirect nature" another factor closely related to optoelectronic properties of the system is the "real-space direct/indirect nature", that is, the real-space overlap between initial and final states involving in optical transition. It is controlled by the specific location of initial and final states, which is here either in between the MoS_2 layers (i.e., in the van der Waals (vdWs) gap) or confined completely within individual MoS_2 layers. Its effects on optoelectronic properties are reflected by for instance the severely reduced transition strength and exciton binding due to spatial separation of electrons and holes abound in some semiconductor heterojunctions with type II band alignment, such as InAs/GaSb quantum well[22] as well as GaAs/AlAs quantum dots.[23,24]

Received: September 27, 2014
Revised: December 24, 2014
Published: January 6, 2015

DOI: 10.1021/nl503717p
Nano Lett. 2015, 15, 949−957

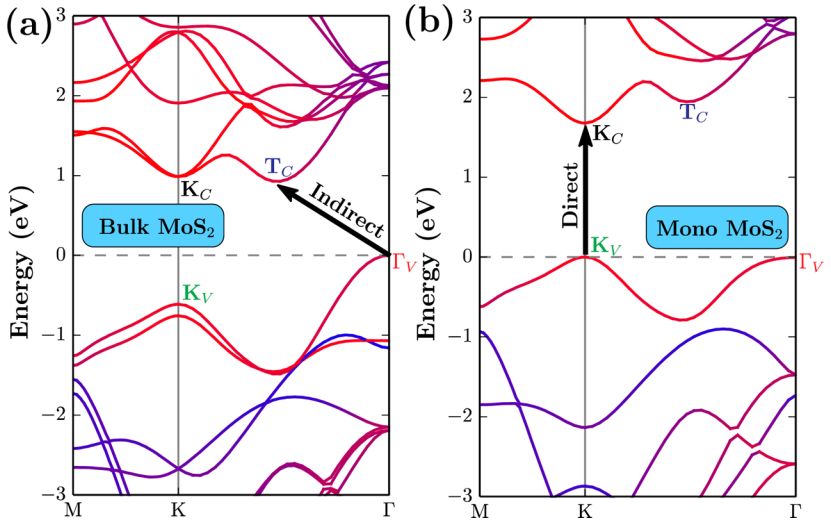

Figure 1. Calculated band structure for MoS_2 of the bulk (a) and the monolayer (b). The band structure has been projected onto constituting atomic species with the blue color representing S and red representing Mo. The band-edge states relevant to optical transition (K_V, K_C, Γ_V, and T_C) are labeled and the band gap transitions are indicated.

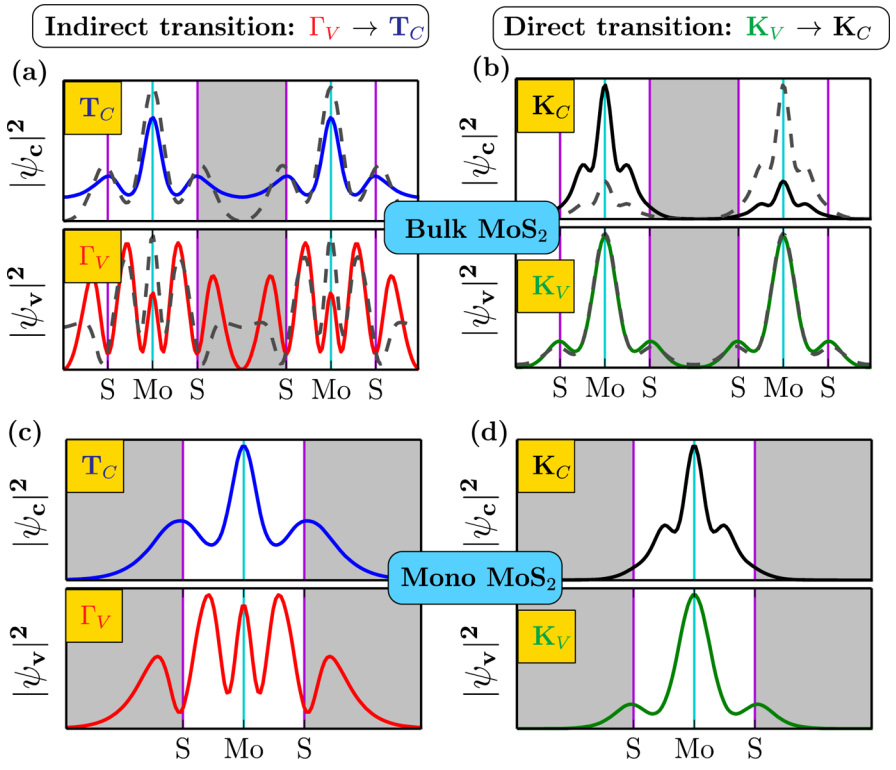

Figure 2. Planar-averaged squared magnitude of wave functions for the relevant band-edge states (as labeled in Figure 1) for MoS_2 of the bulk (upper panels) and the monolayer (lower panels), plotted along the direction perpendicular to the layers. Panels (a,c) refer to the indirect $\Gamma_V \rightarrow T_C$ band gap transition, and panels (b,d) correspond to the direct $K_V \rightarrow K_C$ transition. The positions of Mo and S atoms are marked and the interstitial region outside the sandwich S−Mo−S layers is shown in gray. In (a,b), the second band-edge state (further away from band gap in Figure 1a) is shown with the dark gray dash line.

In this paper, by employing ab initio density functional calculations including the long-range dispersion interaction we analyze the evolution with n of electronic energies and wave functions in the n-ML stack $(MoS_2)_n$ and discover three distinct types of regions with characteristic combination of k-space and real-space direct/indirect nature ("localization prototypes") of band-edge states deciding the optical response of the system. This comparative analysis with different thicknesses is nontrivial as it requires the alignment of the band structures at different n with respect to each other. We do so by considering, in effect, the relative band offsets of different n, via aligning band-edge energies with respect to the averaged electrostatic potential in the vacuum region, thereby establishing common reference to all thicknesses (much as the band offsets calculated for hetertojunctions[25]). Identifying and characterizing these "localization prototypes" is important because they potentially control many aspects of optoelectronic response in the TMDs family, including not only the transition strength and

DOI: 10.1021/nl503717p
Nano Lett. 2015, 15, 949−957

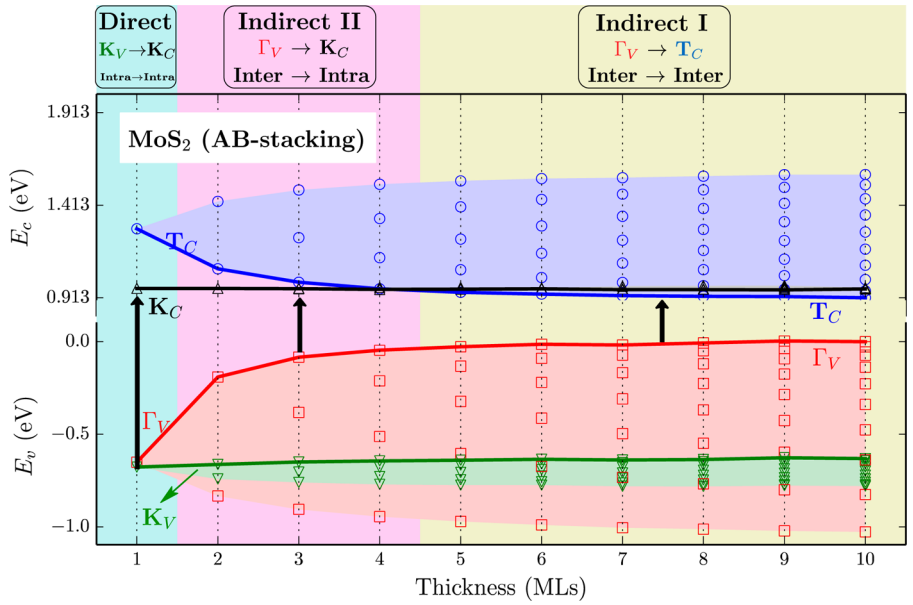

Figure 3. Evolution of various band-edge states (as labeled in Figure 1) of MoS_2 going from multiple-layered films (with the AB-type stacking) to the monolayer. The energy levels corresponding to different band-edges are shown in different colors: Γ_V (red), K_V (green), T_C (blue), and K_C (Black). For each state, the span of energy levels is shaded in the lighter color. The valence band maximum of the Γ_V state at 10 MLs is set to zero. The first *y*-axis tick of the upper panel (conduction bands) refers to the band gap value at 10 MLs. The band gap transitions show three distinct regimes (see text for more detailed description): Indirect I ($\Gamma_V \rightarrow T_C$, in yellow background), Indirect II ($\Gamma_V \rightarrow K_C$, in pink), and Direct ($K_V \rightarrow K_C$, in cyan).

exciton binding as mentioned but also the carrier lifetime, effect of external fields on the electronic states, charge separation across heterojunctions, and so forth. We test our understanding developed here on the nature of band-edge wave functions by designing a simple atomic intercalation model, whereby electron-repelling atoms are selectively placed in the interlayer area so as to deliberately repel those states having a large wave function amplitude at the intercalated sites.

What Controls the Spatial Localization and Momenta of the Band-Edge Absorbing States. Two leading factors are involved here:

(i). Intralayer Localized Vs Interlayer Delocalized States. The physical mechanism governing the evolution of band-edge states with n is intimately related to our understanding of the nature of electronic wave functions in this system having vdWs bonding between layers and covalent bonding within each layer. It is generally known that the electronic wave functions of vdWs system do not extend to the space separating the vdWs units (e.g., interlayer region in layered structures or interatomic region in atomic rare-gas solids) because vdWs bonds are predicated on induced interactions (of fluctuating dipoles) rather than on static charge densities. This is the case in the classic vdWs system of rare-gas solids showing atomically localized states and no bonding charge between atoms.[26] Inspection of the calculated planar-averaged wave function of relevant band-edge states of MoS_2 in Figure 2 shows indeed that the K_V and K_C states made of mainly the Mo *d* and the S p_x and p_y orbitals (Supporting Information Table S1) are atomically localized within each S−Mo−S sandwich layer and do not leak into the interlayer space. When the number of layers n changes, such states behave as "zero confinement states" (Figure 3) in that their band energies are pinned to a constant value. Yet the Γ_V and T_C states made of mainly the Mo *d* and the S p_z orbitals (Supporting Information Table S1) leak notably outside the S−Mo−S layers (Figure 2) showing substantial delocalization in the interlayer region, uncharacteristic of vdWs bonding. The behavior of the band energies of these interlayer extended states with n depicted in Figure 3 shows significant energy variation, in sharp contrast to the pinned "zero confinement states" of K_V and K_C.

(ii). Kinetic-Energy Controlled Quantum Confinement versus Potential-Energy Controlled Band Coupling/Repulsion. The understanding of the evolution of energy levels and interband transitions with n in $(MoS_2)_n$ depends on the physical picture invoked for the pertinent electronic states. Despite of extensive experimental[4−7,20] and theoretical[27−29] studies, it is still unclear whether the physical mechanism underlying the indirect-to-direct band gap transition from $n = \infty$ to $n = 1$ involves the intuitively appealing kinetic-energy controlled quantum confinement effect (hole and electron levels shifting at reduced confinement volumes to lower and higher binding energies, respectively), as generally cited,[4,6,7] or the potential-energy controlled band coupling effect (level repulsion induced by the interlayer coupling potential ΔV).[20] In addition to the first-principle density functional theory calculations, to discern these effects we employ an electronic structure method, "truncated crystal approach" that explicitly neglects the potential-energy controlled band coupling and thus reveal the quantum confinement by mapping the realistic band structure of bulk MoS_2 onto finite-size confined films. The results indicate that different band-edge states behave differently: the T_C state is controlled solely by quantum confinement and Γ_V is controlled by both quantum confinement as well as band repulsion, whereas K_C and K_V are intrinsically localized states and do not respond to kinetic-energy confinement with reduced thickness.

Classification of Individual Band-Edge States in Terms of Their Wave Function Features for MoS_2. We start by classifying the band-edge states controlling band gap transitions, including Γ_V, T_C, K_V, and K_C as mentioned above. Figure 2 shows their planar-averaged wave functions squared plotted perpendicular to the S−Mo−S layers for both

DOI: 10.1021/nl503717p
Nano Lett. 2015, 15, 949−957

bulk and monolayer. The main features of these band-edge states, including atomic orbital character, spatial distribution, and degree of coupling between adjacent layers, are summarized in Supporting Information Table S1. These results are generally consistent with previous first-principle calculations.[28,30,31]

(i) States involved in the direct $K_V \rightarrow K_C$ transition, that is, the intralayer localized states. In this grouping, both initial (K_V) and final (K_C) states originate from *d* states of the centered Mo and p_x, p_y state of the sideward S atoms (Supporting Information Table S1). As shown in Figure 2d, their corresponding wave functions in monolayer MoS_2 are localized within the sandwich S−Mo−S layer with almost no (K_C) or tiny (K_V) leakage outside the layer. Thus, the K_V and K_C states can be classified as the "intralayer localized" states. The rather localized feature of these states results in small wave function overlap in bulk MoS_2 (Figure 2b) and thus weak coupling/interaction between adjacent layers. This is responsible for the nearly degenerate bands of K_C and extremely small (~200 meV) band splitting of K_V in the bulk (Figure 1a).

(ii) States involved in the indirect $\Gamma_V \rightarrow T_C$ transition, that is, the interlayer delocalized states. Here, both initial (Γ_V) and final (T_C) states are composed of a large portion of the p_z state of the sideward S atoms (Supporting Information Table S1) and thus have extended wave functions with substantial leakage outside the S−Mo−S layer (Figure 2c). Especially for the Γ_V state (the lower panel of Figure 2c), we can clearly see a strong peak of wave function distribution in the region outside the layer. We thus classify the Γ_V and T_C states as the "interlayer delocalized" states. As shown in Figure 2a, in bulk MoS_2 these delocalized states show much stronger coupling between adjacent layers compared with the intralayer localized K_V and K_C states. In the lower panel of Figure 2a, it can be seen that the strong interlayer coupling of the Γ_V state results in bonding (dark gray, corresponding to the second lower band of Γ_V in Figure 1a) and antibonding (red, corresponding to the band edge of Γ_V in Figure 1a) like charge distribution. This strong interlayer coupling explains the extremely large (>1 eV) band splitting inside the valence bands at Γ_V (Figure 1a).

Engineering the Band Structure of MoS_2 by Repelling the Interlayer Delocalized States via Atomic Intercalation. The existence of interlayer delocalized states Γ_V and T_C in MoS_2 offers an opportunity to control its electronic properties by intercalating in the interstitial area between layers some electron-repelling atoms or ions. The situation is analogous to the wave function of conduction band X_C in silicon and III−V zinc blende semiconductors that has its maximum amplitude in the interstitial space rather than on the covalent bond,[32,33] so intercalation of small inert atoms, such as He has been shown to effectively repel the energy of the X_C state in preference to the states such as Γ_C that do not have large interstitial amplitudes of wave function.[33]

To illustrate such behavior (rather than to find the practical intercalates that have large solubility) we calculated the band structure for bulk MoS_2 with the He intercalated as shown in Figure 4. We consider the configuration in which the He atoms are placed on top of the center of (buckled) honeycombs (Figure 4a), and all the equivalent sites enforced by symmetry are occupied by He. Total energy relaxation is performed for all the He atoms with the fixed structural parameters of MoS_2. In agreement with expectations, the energy of the T_C state being an interlayer delocalized state is raised as the result of placing the electron repelling He atoms in the interlayer region. This

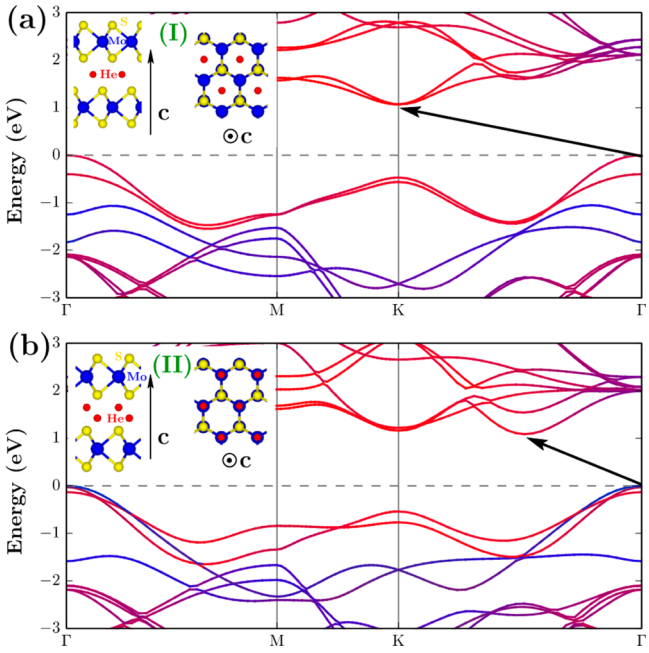

Figure 4. Calculated band structures of bulk MoS_2 with He atoms intercalated into the interlayer area. The subplot (a) and (b) correspond to different patterns of He intercalating, I and II (as indicated in the insets), respectively. In the pattern I, He atoms are located on top of the center of (buckled) honeycombs, and in the pattern II He atoms are put on top of Mo/S sites. Similar to Figure 1, the band structures are projected onto constituting atomic species.

level is effectively shifted above that of K_C being an intralayer localized state, confirming the idea that intercalation can selectively shift energy levels in proportion to their wave function amplitudes at the intercalated sites. Another interlayer delocalized state, the Γ_V state, is also repelled by He atoms to the lower binding energy but still higher than that of K_V in the current model, leading to an indirect band bap from Γ_V to K_C. These clearly indicate that the electronic structures of layered group-VIB TMDs could be effectively modified by purposely controlling the interlayer delocalized states via intercalation. Note that an alternative pattern of He intercalation in Figure 4b where He atoms are located on top of Mo/S sites does not exhibit a remarkable repelling effect, where the indirect band bap from Γ_V to T_C preserved. Thus, not all geometrical patterns of intercalation result in a maximal effect, so this is indeed a design problem.

Evolution of Band-Edge States with the Layer Thickness and Distinct Localization Prototypes for MoS_2. To explore how various band-edge states evolve with the layer thickness, we calculated the band structures of multiple-layered stack $(MoS_2)_n$ with n = 1−10 MLs (see Supporting Information Figure S1). After aligning band energy levels at different layer thicknesses (see Computational Methods) we obtain the evolution of the band-edge states relevant to band gap transition (Γ_V, T_C, K_V, and K_C) for the stack of the AB-type (see Computational Methods) as shown in Figure 3 (see Supporting Information Figure S3b for the result of the AA-type stacking). We find that the interlayer delocalized Γ_V and T_C states show, as n is gradually reduced, a common behavior: the lower bound of energy level groups increases in energy and the higher bound decreases, eventually converging to a single value at the monolayer. In contrast, the intralayer localized K_V and K_C states exhibit narrow or nearly zero energy

DOI: 10.1021/nl503717p
Nano Lett. 2015, 15, 949−957

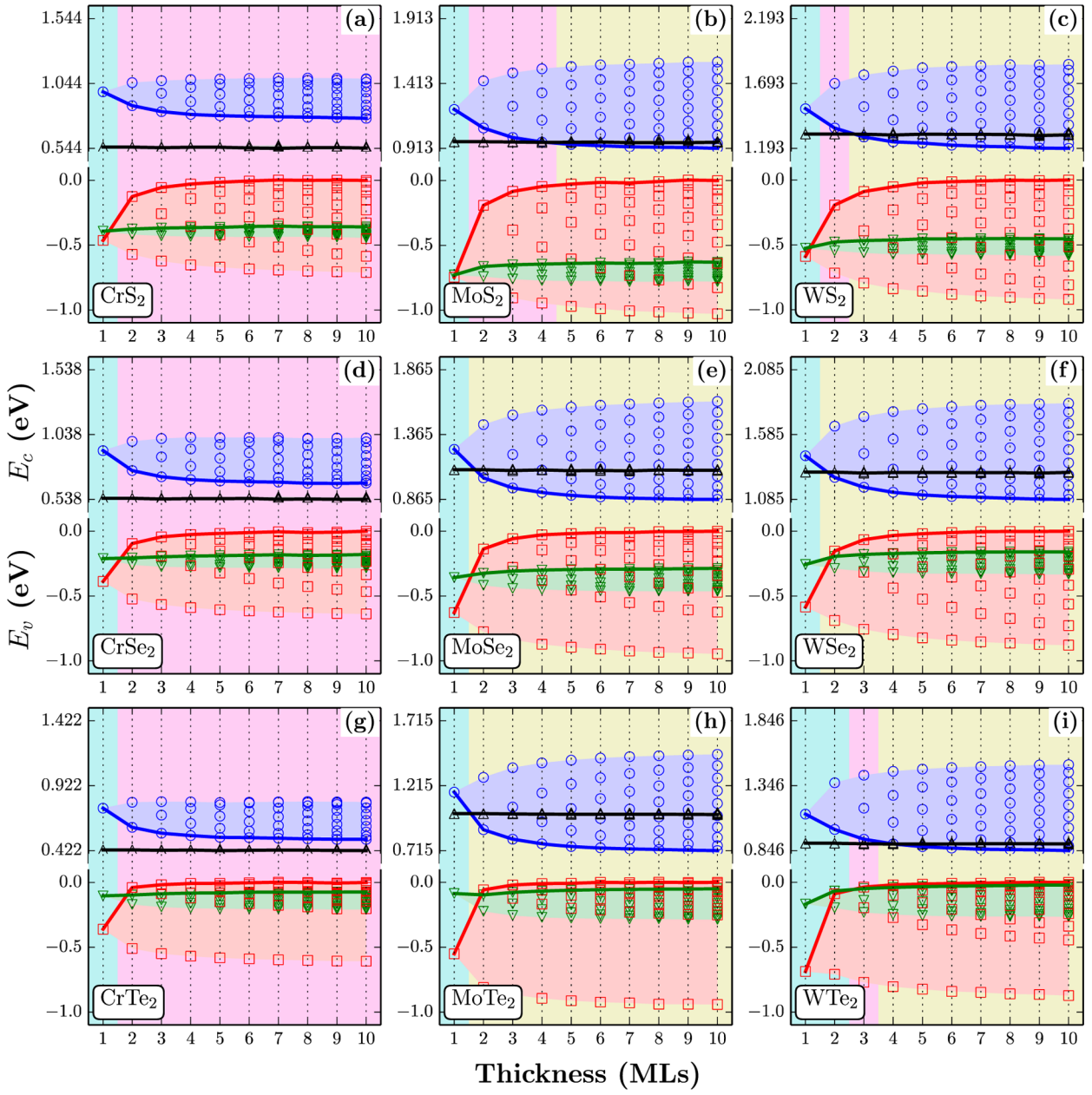

Figure 5. Evolution of various band-edge states going from multiple-layered films (with AB-stacking) to the monolayer for all the group-VIB TMDs MX_2 (M = Cr, Mo, W and X = S, Se, Te). Similar to Figure 3, different band-edges are shown in different colors: T_C (blue), K_C (Black), Γ_V (red), and K_V (green) and different regimes of band gap transitions are indicated by different background colors: Indirect I ($\Gamma_V \rightarrow T_C$, in yellow), Indirect II ($\Gamma_V \rightarrow K_C$, in pink), and Direct ($K_V \rightarrow K_C$, in cyan).

span. Note that with the inclusion of spin−orbit coupling (see Supporting Information Figure S2), while the evolution profiles of Γ_V, T_C, and K_C states do not change much, the K_V state is split into the lower and upper spin-split groups, each having an even narrower span than 50 meV. The narrow span width of the upper spin-split group, accompanying the nearly zero span width of the K_C state, leads to the nearly constant energy gap of the direct $K_V \rightarrow K_C$ transition with the decreasing layer thickness. Different evolution behavior of these two groups of states (interlayer delocalized and intralayer localized) leads to specific crossings between them, and thus the following three distinct regimes with characteristic localization prototypes of band-edge states deciding the optical response of the system:

(i) For the thick $n > 4$ layers, we encounter the *k*-space indirect optical transition connecting in momentum-space an initial valence state Γ_V with a final conduction state T_C (Indirect I, yellow background), both exhibiting delocalized feature in the interlayer region. The charge distribution of photon-excited carriers in this regime is hence direct in real-space but indirect in *k*-space.

(ii) For the layers with intermediate thickness $1 < n < 5$, the transition is indirect in *k*-space and connects an initial state Γ_V that is delocalized in the interlayer region with a final state K_C that is localized within the layers (Indirect II, pink background). The charge distribution of carriers in this regime is thus indirect in real-space, as well as in *k*-space.

(ii) Finally, for the $n = 1$ monolayer the transition is *k*-space direct, connecting an initial state K_V with a final state K_C (direct, cyan background), both being localized in real-space

DOI: 10.1021/nl503717p
Nano Lett. 2015, 15, 949−957

within the layer. The charge distribution of carriers is thus direct in both *k*-space and real-space.

Evolution of Band-Edge States with the Layer Thickness for Different M = Cr, Mo, W and X = S, Se, Te. We next extended the above calculations on MoS_2 to more other group-VIB TMDs. Similar to that of MoS_2, the multiple-layered films are constructed based on the ground-state bulk structure of the 2H polytype, and fully optimized by the total-energy minimization. The evolutions of relevant band-edge states with reduced layer thickness for all the MX_2 (M = Cr, Mo, W and X = S, Se, Te) in the AB-type stacking are shown in Figure 5 (see Supporting Information Figure S3 for the results of the AA-type stacking).

While the general classification of distinct regimes with characteristic localization prototypes of band-edge states resembles to that of MoS_2, the specific regimes and corresponding demarcation *n* values can be different in different materials. Particularly, when walking through different MX_2 we have the following observations: (i) For Cr-series materials, the energy span widths of all the band-edge states are much narrower. This is attributed to the weaker coupling between adjacent layers, which results from the relatively larger interlayer distance caused by the smaller size of Cr. (ii) With the exception of $MoTe_2$, where the direct band gap ($K_V \rightarrow K_C$, cyan background) transition has emerged starting from the bilayer, all the other materials only exhibit direct transition at the monolayer. (iii) For the Cr-series materials, there appear only two regimes, the Indirect II ($\Gamma_V \rightarrow K_C$, pink background) and Direct ($K_V \rightarrow K_C$, cyan background). This results from the lower energy of K_C than that of T_C in the whole thickness range because of the narrower energy span width of T_C. (iv) For $MoSe_2$, $MoTe_2$, and WSe_2, there exist another two regimes, the Indirect I ($\Gamma_V \rightarrow T_C$, yellow background) and Direct ($K_V \rightarrow K_C$, cyan background). This is caused by the much higher energy of K_C than that of the T_C lower boundary, becoming the band edge only at the monolayer. (v) In the same column ranging from sulfide, selenide to telluride, the energy difference between K_V and the upper boundary of Γ_V becomes smaller and smaller. The effect maximizes at the tellurides, where their energy levels almost coincide.

Evolution of Layer−Layer Binding Energies with the Layer Thickness for MoX_2 (X = S, Se, Te). In addition to the evolution of band energy levels, we also explored how layer−layer binding energies evolve with the decreasing layer thickness, as shown in Figure 6 for the Mo-series materials. The layer−layer binding energy of multiple (*n*) layered material (E_b, in meV/layer) is defined via $E_b = E_n/n - E_1$, where *n* is the number of layers, E_n and E_1 are the total energy of *n* layers and monolayer, respectively. Two observations can be drawn from the results: (i) at the same *n*, E_b increases from MoS_2, $MoSe_2$ to $MoTe_2$; (ii) E_b exhibits an asymptotic decrease when the number of layers is reduced. Both of them can be rationalized in terms of the variation of the average interaction area for the layered vdWs system, as demonstrated by Björkman et al. in ref 34. Note that the variation range of E_b (<350 meV) is much smaller than the band energy span widths of the interlayer delocalized Γ_V and T_C states (approaching 1 eV as in Figure 3). The implication is that in the layered vdWs materials the global energetics of the system may be less affected by the interlayer coupling, compared with the situation of some particular electronic states. This is understandable because the former is to be weighted by all the occupied electronic states, whereas the latter might be significantly enhanced by the direct wave function overlapping between adjacent layers (as in Figure 2a).

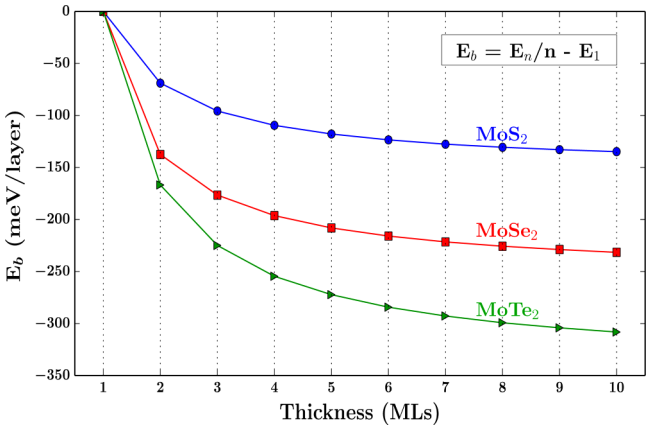

Figure 6. Evolution of layer−layer binding energies (E_b, in meV/layer) with the increased layer thickness for the Mo-series materials, MoX_2 (X = S, Se, Te).

Wave Function Overlap of Initial and Final States as a Measure of Optical Activity of Distinct Regimes with Different Prototype Transitions. To probe the potential effects of distinct regimes with characteristic localization prototypes of band-edge states on optical activities of the system, we calculated the wave function overlap between CBM and VBM, $\int|\psi_C||\psi_V|dr^3$, which is closely relevant to the intensity of optical transition, carrier lifetime exciton binding, and so forth. Its evolution from multiple-layered films to the monolayer for all the MX_2 is shown in Figure 7. As expected the strongest overlap occurs at the Direct ($K_V \rightarrow K_C$, cyan background) regime, because of the direct nature of initial and final states in both *k*-space and real space. As to the Indirect I ($\Gamma_V \rightarrow T_C$, yellow background) regime, although the initial and final states are indirect in *k*-space, the direct nature of them in real space gives rise to the relatively strong overlap magnitude that is almost independent of the layer thickness. The weakest overlap happens in the Indirect II ($\Gamma_V \rightarrow K_C$, pink background) regime accompanying with complicated oscillation behavior, as the result of the indirect nature of initial and final states in real space. These results are generally uniform for all the MX_2 and consistent with our classification of various band-edge states (Supporting Information Table S1) and division of distinct regimes with different prototype transitions (Figure 5).

What Causes the Indirect-to-Direct Band Gap Transition: Quantum Confinement versus Interlayer Coupling. Because the K_C and K_V states are intralayer localized due to the specific atomic orbitals composing them (Supporting Information Table S1), they are pinned to a fixed energy when the layer thickness is reduced, not experiencing substantial change in energy. As for the interlayer delocalized T_C and Γ_V states, the dependence of their energy on the layer thickness (the blue and red solid line in Figure 3, respectively) could intuitively suggest the dominating physical factor being quantum confinement effect, where the energy level of nanostructures increases as the result of increased kinetic energy when the size of nanostructures reduced.[35] However, if one notes also in Figure 3 the upper boundary of T_C and the lower boundary of Γ_V, one realizes that this picture can also be interpreted by the simple two-level band coupling model, where the interlayer coupling potential ΔV mutually repels the two states when *n* gradually increased starting from 1, resulting in

DOI: 10.1021/nl503717p
Nano Lett. 2015, 15, 949−957

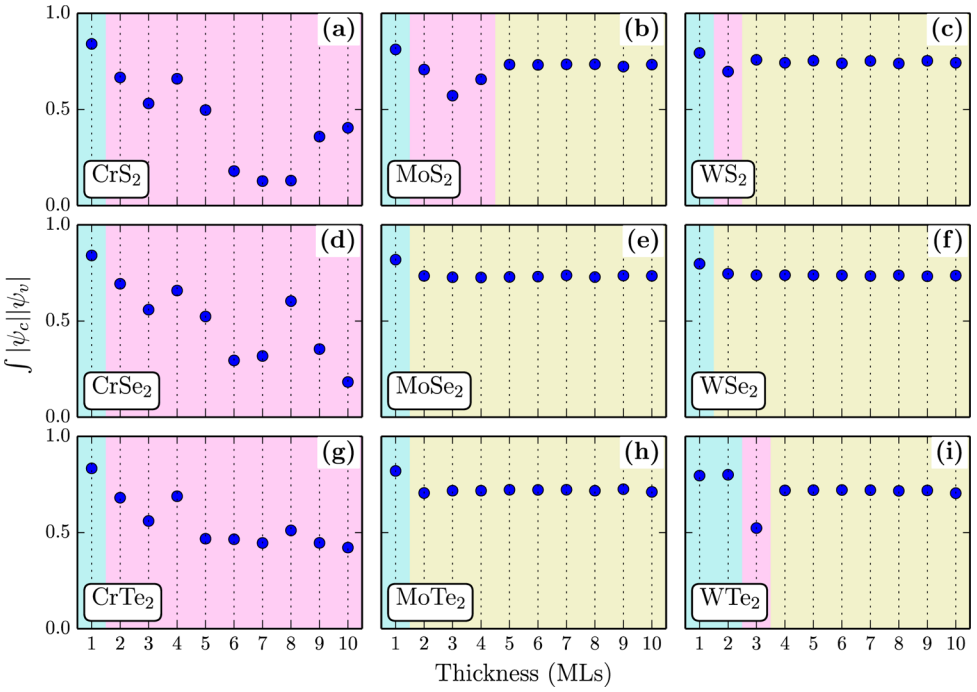

Figure 7. Evolution of the wave function overlap $\int|\psi_C||\psi_V|dr^3$ between conduction and valence band-edge states going from multiple-layered films to the monolayer for all the group-VIB TMDs MX_2 (M = Cr, Mo, W and X = S, Se, Te) with the AB-type stacking. As in Figure 5, different regimes of band gap transitions are indicated by different background colors: Indirect I ($\Gamma_V \rightarrow T_C$, in yellow), Indirect II ($\Gamma_V \rightarrow K_C$, in pink), and Direct ($K_V \rightarrow K_C$, in cyan).

the uniform shape (with the lower bonding-like and higher antibonding like boundary) seen in Figure 3.

To reveal the underlying mechanism, we employed the truncated crystal (TC) approach[36,37] to evaluate the energy levels of finite-size multiple-layered films resulted solely from the kinetic-energy controlled quantum confinement. In this approach, one converts the three-dimensional realistic band structure of the bulk material to the quantized energy levels of the two-dimensional film by determining for each film thickness the wave vectors $\{K\}$ at which the wave function vanishes at the film boundary. This approach deliberately neglects the potential-energy controlled band coupling in the film (by using precisely the eigenstates of bulk material), and exactly retains kinetic-energy effect (while avoiding the parabolic approximation that is often used along with the simple quantum confinement treatment such as effective mass approximation).[36,37]

Figure 8 shows the results for MoS_2 from the TC approach (open symbols and dash lines) and compares them with the corresponding results from direct density functional theory calculations of the films (close symbols and solid lines). Both AB-type (a) and AA-type (b) stackings are considered. We first see that the TC results reproduce the pinned behavior of the intralayer localized K_C and K_V states as resulting from the nearly dispersionless bulk band structure along the z direction. For the T_C state, the TC results agree closely with the direct calculations for both AB-type and AA-type stacking, which clearly shows that the quantum confinement effect is indeed responsible for its evolution with the layer thickness. However, this is not the case for the Γ_V state, where significant deviation between the TC results and direct calculations is observed, especially during the change from bilayer to monolayer. This indicates that the quantum confinement itself is not enough to explain the Γ_V evolution, implying that another effect, interlayer

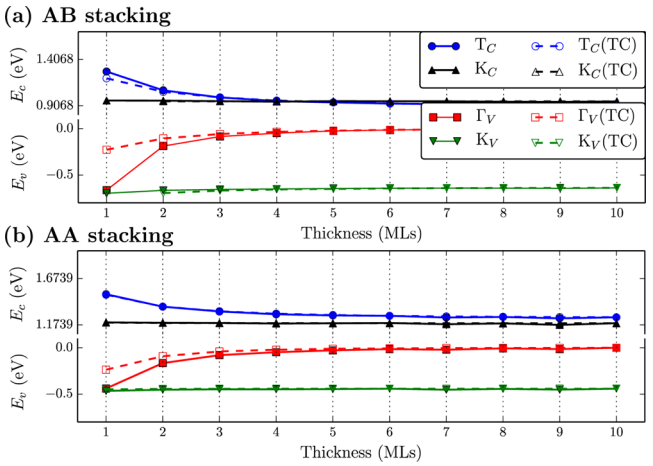

Figure 8. Comparison between direct calculations (close symbols and solid lines) and the results from the truncated crystal approach (open symbols and dash lines) for the evolution of various band-edge states with the layer thickness of the MoS_2 films in (a) AB-stacking and (b) AA-stacking. Different from Figure 3, here only the lower boundaries of conduction-band edges and the upper boundaries of valence-band edges, which dominate the band gap formation, are plotted.

coupling, plays an import role in its evolution. The showing evolution shape is thus as the result of the competition of these two effects. This conclusion is further supported by the results with the varied layer−layer distances, as shown in Supporting Information Figure S4 for the AA-type stacking of MoS_2: with the increased interlayer coupling (by decreasing the layer−layer distance), the evolutions of the interlayer delocalized Γ_V and T_C states exhibit more dramatic changes. Meanwhile, the truncated crystal results show more remarkable deviation from direct calculations, clearly evidencing the incapability of the quantum

DOI: 10.1021/nl503717p
Nano Lett. 2015, 15, 949−957

confinement effect being responsible for the realistic evolution profiles.

Conclusion. We presented via first-principle density functional theory calculations including the long-range dispersion interaction a study of the evolution of electronic structure for the family of layered group-VIB transition metal dichalcogenides with varied number n of the $(MX_2)_n$ stack as well as different combinations of cation and anion species (M = Cr, Mo, W and X = S, Se, Te). The band-edge states relevant to optical transition at different layer thicknesses are classified in terms of the criteria of both k-space direct (i.e., momentum conserving) and real-space direct (i.e., carrier distribution) natures. This allows us to identify a series of characteristic combination of k-space and real-space direct/indirect nature ("localization prototypes") of the band-edge states determining the optical response of the system. We find that in MoS_2 when the layer thickness decreased, there appear three distinct regimes of optical transition determined by different localization prototypes of band-edge states: (i) for the thick layers with $n > 4$ the transition is direct in real-space but indirect in k-space; (ii) for the layers with intermediate thickness $1 < n < 5$ the transition is indirect in both real-space and k-space; (iii) for the $n = 1$ monolayer the transition is direct in both real-space and k-space.

While generally the transition from indirect to direct band gap occurs in all the MX_2 when going from multiple-layered films to the monolayer, we find that the specific distinct regimes with characteristic localization prototypes of band-edge states show strong material dependence. This implies a wide tunability range of the optoelectronic properties of multiple-layered MX_2. Identifying these localization prototypes and resulting distinct regimes of optical transitions in the current layered system play an important role in understanding the evolution of various optoelectronic behaviors as the function of the layer thickness, including the intensity of optical transitions, binding energy and lifetime of excitons, effect of external fields on the states, charge separation across heterojunctions, response of the system to intercalation between the layers, etc.

Computational Methods. First-principle density functional theory (DFT) calculations were performed using the plane wave basis, projected augmented wave potentials[38] and generalized gradient approximation (GGA) with the Perdew–Burke–Ernzerhof exchange-correlation functional,[39] as implemented in the Vienna Ab initio simulation package.[40,41] We used the k-point samplings in the Brillouin zone of $22 \times 22 \times 5$ for the bulk material, $22 \times 22 \times 2$ for the thinner layers (with the thickness $l = 1$–4 MLs), and $22 \times 22 \times 1$ for the thicker layers ($l > 4$ MLs). The convergence threshold of self-consistent iteration was set to 10^{-6} eV/atom. The evolution of electronic energy levels with the layer thickness was obtained by aligning the band structures at different thicknesses with respect to the averaged electrostatic potential in the vacuum region. We included the interlayer vdWs interaction in the current layered system by using the DFT-D2 approach (via adding a semiempirical dispersion potential to the conventional DFT total energy).[42] For all the MX_2 involved in this work, we fully optimized the lattice parameters and cell-internal atomic positions until the change in total energy between two steps of ionic relaxation is less than 10^{-4} eV/atom. The ground-state structure of group-VIB TMDs is known to adopt the 2H polytype, where the metal M atom has trigonal prismatic coordination within the X–M–X sandwich layer and two sandwich layers in each unit cell are arranged in the AB-type stacking (the M atoms of the one layer directly above the X atoms of the adjacent layer).[2] With the vdWs interaction included the optimized lattice parameters of known MX_2 show reasonable agreement with the available experimental results. For completeness, we considered not only currently known TMDs (MoS_2, $MoSe_2$, $MoTe_2$, WS_2, WSe_2),[1−3] but also other hypothetical, yet unsynthesized TMDs (M = Cr, Mo, W and X = S, Se, Te). In addition to the ground-state AB-type stacking, the metastable AA-type stacking case (one layer directly above the adjacent layer) is also considered. It should be pointed out that although usually the standard DFT-GGA calculations underestimate the band gap of materials, this situation does not affect the main results we obtained here. The effect of spin–orbit coupling on the evolution of band-edge states is examined in the prototype material MoS_2 (see Supporting Information Figure S2). Consistent with previous calculations,[31,43,44] the predominant effect of spin–orbit coupling is that for a full range of layer thicknesses the valence band edges at the K point are split into two components, with a splitting magnitude of 150–200 meV. This does not influence the main findings of this work, and thus the spin–orbit coupling is reasonably excluded by considering computational cost. We employed the truncated crystal approach[36,37] to evaluate the energy levels of finite-size multiple-layered films resulted solely from the kinetic-energy controlled quantum confinement.

■ ASSOCIATED CONTENT

Supporting Information

Additional information including characteristics of various band-edge states of MoS_2, band structures of multiple-layered MoS_2 films, as well as evolution of various band-edge states with the inclusion of spin–orbit coupling, for the AA-type stacking and with the changed layer–layer distance. This material is available free of charge via the Internet at http://pubs.acs.org.

■ AUTHOR INFORMATION

Corresponding Authors

*E-mail: lijun_zhang@jlu.edu.cn (L.Z.).
*E-mail: Alex.Zunger@colorado.edu (A.Z.).

Notes

The authors declare no competing financial interest.

■ ACKNOWLEDGMENTS

Work at CU Boulder was supported by Office of Science, Basic Energy Science, Materials Sciences and Engineering Division under Grant DE-FG02-13ER46959. Work at Jilin University was supported by National Natural Science Foundation of China under Grant No. 11404131. L.Z. is grateful to S. H. Wei, L. Yu, J. Kang, J. W. Luo, and X. Zhang for helpful discussion.

■ REFERENCES

(1) Wang, Q. H.; Kalantar-Zadeh, K.; Kis, A.; Coleman, J. N.; Strano, M. S. Electronics and optoelectronics of two-dimensional transition metal dichalcogenides. *Nat. Nanotechnol.* **2012**, *7*, 699–712.

(2) Chhowalla, M.; Shin, H. S.; Eda, G.; Li, L.-J.; Loh, K. P.; Zhang, H. The chemistry of two-dimensional layered transition metal dichalcogenide nanosheets. *Nat. Chem.* **2013**, *5*, 263–275.

(3) Eda, G.; Maier, S. A. Two-Dimensional Crystals: Managing Light for Optoelectronics. *ACS Nano* **2013**, *7*, 5660–5665.

(4) Mak, K. F.; Lee, C.; Hone, J.; Shan, J.; Heinz, T. F. Atomically Thin MoS_2: A New Direct-Gap Semiconductor. *Phys. Rev. Lett.* **2010**, *105*, 136805.

DOI: 10.1021/nl503717p
Nano Lett. 2015, 15, 949–957

(5) Tongay, S.; Zhou, J.; Ataca, C.; Lo, K.; Matthews, T. S.; Li, J.; Grossman, J. C.; Wu, J. Thermally Driven Crossover from Indirect toward Direct Bandgap in 2D Semiconductors: $MoSe_2$ versus MoS_2. *Nano Lett.* **2012**, *12*, 5576−5580.
(6) Jin, W.; Yeh, P.-C.; Zaki, N.; Zhang, D.; Sadowski, J. T.; Al-Mahboob, A.; van der Zande, A. M.; Chenet, D. A.; Dadap, J. I.; et al. Direct Measurement of the Thickness-Dependent Electronic Band Structure of MoS2 Using Angle-Resolved Photoemission Spectroscopy. *Phys. Rev. Lett.* **2013**, *111*, 106801.
(7) Zhang, Y.; Chang, T.-R.; Zhou, B.; Cui, Y.-T.; Yan, H.; Liu, Z.; Schmitt, F.; Lee, J.; Moore, R.; et al. Direct observation of the transition from indirect to direct bandgap in atomically thin epitaxial $MoSe_2$. *Nat. Nanotechnol.* **2014**, *9*, 111−115.
(8) Kośmider, K.; Fernández-Rossier, J. Electronic properties of the MoS_2-WS_2 heterojunction. *Phys. Rev. B* **2013**, *87*, 075451.
(9) Terrones, H.; López-Urías, F.; Terrones, M. Novel hetero-layered materials with tunable direct band gaps by sandwiching different metal disulfides and diselenides. *Sci. Rep.* **2013**, *3*, 1549.
(10) Geim, A. K.; Grigorieva, I. V. Van der Waals heterostructures. *Nature* **2013**, *499*, 419−425.
(11) Komsa, H.-P.; Krasheninnikov, A. V. Electronic structures and optical properties of realistic transition metal dichalcogenide heterostructures from first principles. *Phys. Rev. B* **2013**, *88*, 085318.
(12) Conley, H. J.; Wang, B.; Ziegler, J. I.; Haglund, R. F.; Pantelides, S. T.; Bolotin, K. I. Bandgap Engineering of Strained Monolayer and Bilayer MoS_2. *Nano Lett.* **2013**, *13*, 3626−3630.
(13) Zhu, C. R.; Wang, G.; Liu, B. L.; Marie, X.; Qiao, X. F.; Zhang, X.; Wu, X. X.; Fan, H.; Tan, P. H.; et al. Strain tuning of optical emission energy and polarization in monolayer and bilayer MoS_2. *Phys. Rev. B* **2013**, *88*, 121301.
(14) Feng, J.; Qian, X.; Huang, C.-W.; Li, J. Strain-engineered artificial atom as a broad-spectrum solar energy funnel. *Nat. Photonics* **2012**, *6*, 866−872.
(15) Johari, P.; Shenoy, V. B. Tuning the Electronic Properties of Semiconducting Transition Metal Dichalcogenides by Applying Mechanical Strains. *ACS Nano* **2012**, *6*, 5449−5456.
(16) He, K.; Poole, C.; Mak, K. F.; Shan, J. Experimental Demonstration of Continuous Electronic Structure Tuning via Strain in Atomically Thin MoS_2. *Nano Lett.* **2013**, *13*, 2931−2936.
(17) Peelaers, H.; Van de Walle, C. G. Effects of strain on band structure and effective masses in MoS_2. *Phys. Rev. B* **2012**, *86*, 241401.
(18) Qi, J.; Li, X.; Qian, X.; Feng, J. Bandgap engineering of rippled MoS_2 monolayer under external electric field. *Appl. Phys. Lett.* **2013**, *102*, 173112−173112−4.
(19) Wu, S.; Ross, J. S.; Liu, G.-B.; Aivazian, G.; Jones, A.; Fei, Z.; Zhu, W.; Xiao, D.; Yao, W.; et al. Electrical tuning of valley magnetic moment through symmetry control in bilayer MoS_2. *Nat. Phys.* **2013**, *9*, 149−153.
(20) Han, S. W.; Kwon, H.; Kim, S. K.; Ryu, S.; Yun, W. S.; Kim, D. H.; Hwang, J. H.; Kang, J.-S.; Baik, J.; et al. Band-gap transition induced by interlayer van der Waals interaction in MoS_2. *Phys. Rev. B* **2011**, *84*, 045409.
(21) Zhao, W.; Ribeiro, R. M.; Toh, M.; Carvalho, A.; Kloc, C.; Castro Neto, A. H.; Eda, G. Origin of Indirect Optical Transitions in Few-Layer MoS_2, WS_2, and WSe_2. *Nano Lett.* **2013**, *13*, 5627−5634.
(22) Bastard, G.; Mendez, E. E.; Chang, L. L.; Esaki, L. Exciton binding energy in quantum wells. *Phys. Rev. B* **1982**, *26*, 1974−1979.
(23) Rorison, J. M. Excitons in type-II quantum-dot systems: A comparison of the GaAs/AlAs and InAs/GaSb systems. *Phys. Rev. B* **1993**, *48*, 4643−4649.
(24) Franceschetti, A.; Zunger, A. Quantum-confinement-induced Γ→X transition in GaAs/AlGaAs quantum films, wires, and dots. *Phys. Rev. B* **1995**, *52*, 14664−14670.
(25) Van de Walle, C. G. Band lineups and deformation potentials in the model-solid theory. *Phys. Rev. B* **1989**, *39*, 1871−1883.
(26) Gans, W.; Boeyens, J. C. A. *Intermolecular Interactions*; Springer Science & Business Media: New York, 1998.
(27) Kuc, A.; Zibouche, N.; Heine, T. Influence of quantum confinement on the electronic structure of the transition metal sulfide TS_2. *Phys. Rev. B* **2011**, *83*, 245213.
(28) Ellis, J. K.; Lucero, M. J.; Scuseria, G. E. The indirect to direct band gap transition in multilayered MoS2 as predicted by screened hybrid density functional theory. *Appl. Phys. Lett.* **2011**, *99*, 261908−261908−3.
(29) Cappelluti, E.; Roldán, R.; Silva-Guillén, J. A.; Ordejón, P.; Guinea, F. Tight-binding model and direct-gap/indirect-gap transition in single-layer and multilayer MoS_2. *Phys. Rev. B* **2013**, *88*, 075409.
(30) Coehoorn, R.; Haas, C.; Dijkstra, J.; Flipse, C. J. F.; de Groot, R. A.; Wold, A. Electronic structure of $MoSe_2$, MoS_2, and WSe_2. I. Band-structure calculations and photoelectron spectroscopy. *Phys. Rev. B* **1987**, *35*, 6195−6202.
(31) Cheiwchanchamnangij, T.; Lambrecht, W. R. L. Quasiparticle band structure calculation of monolayer, bilayer, and bulk MoS_2. *Phys. Rev. B* **2012**, *85*, 205302.
(32) Rompa, H. W. A. M.; Schuurmans, M. F. H.; Williams, F. Predicted Modifications in the Direct and Indirect Gaps of Tetrahedral Semiconductors. *Phys. Rev. Lett.* **1984**, *52*, 675−678.
(33) Wood, D. M.; Zunger, A.; de Groot, R. Electronic structure of filled tetrahedral semiconductors. *Phys. Rev. B* **1985**, *31*, 2570−2573.
(34) Björkman, T.; Gulans, A.; Krasheninnikov, A. V.; Nieminen, R. M. van der Waals Bonding in Layered Compounds from Advanced Density-Functional First-Principles Calculations. *Phys. Rev. Lett.* **2012**, *108*, 235502.
(35) Yu, P.; Cardona, M. *Fundamentals of Semiconductors: Physics and Materials Properties*; Springer: New York, 2010.
(36) Zhang, S. B.; Yeh, C.-Y.; Zunger, A. Electronic structure of semiconductor quantum films. *Phys. Rev. B* **1993**, *48*, 11204−11219.
(37) Franceschetti, A.; Zunger, A. GaAs quantum structures: Comparison between direct pseudopotential and single-band truncated-crystal calculations. *J. Chem. Phys.* **1996**, *104*, 5572−5578.
(38) Kresse, G.; Joubert, D. From ultrasoft pseudopotentials to the projector augmented-wave method. *Phys. Rev. B* **1999**, *59*, 1758−1775.
(39) Perdew, J. P.; Burke, K.; Ernzerhof, M. Generalized Gradient Approximation Made Simple. *Phys. Rev. Lett.* **1996**, *77*, 3865−3868.
(40) Kresse, G.; Hafner, J. Ab initio molecular dynamics for liquid metals. *Phys. Rev. B* **1993**, *47*, 558−561.
(41) Kresse, G.; Furthmüller, J. Efficiency of ab-initio total energy calculations for metals and semiconductors using a plane-wave basis set. *Comput. Mater. Sci.* **1996**, *6*, 15−50.
(42) Grimme, S. Semiempirical GGA-type density functional constructed with a long-range dispersion correction. *J. Comput. Chem.* **2006**, *27*, 1787−1799.
(43) Zhu, Z. Y.; Cheng, Y. C.; Schwingenschlögl, U. Giant spin-orbit-induced spin splitting in two-dimensional transition-metal dichalcogenide semiconductors. *Phys. Rev. B* **2011**, *84*, 153402.
(44) Molina-Sánchez, A.; Sangalli, D.; Hummer, K.; Marini, A.; Wirtz, L. Effect of spin-orbit interaction on the optical spectra of single-layer, double-layer, and bulk MoS_2. *Phys. Rev. B* **2013**, *88*, 045412.

DOI: 10.1021/nl503717p
Nano Lett. 2015, 15, 949−957